Size-Dependent Electroporation of Dye-Loaded Polymer Nanoparticles for Efficient and Safe Intracellular Delivery

Sylvie Egloff, Anne Runser, Andrey Klymchenko, Andreas Reisch

Size-Dependent Electroporation of Dye-Loaded Polymer Nanoparticles for Efficient and Safe Intracellular Delivery

Sylvie Egloff, Anne Runser, Andrey Klymchenko,* Andreas Reisch*

Université de Strasbourg, CNRS, Laboratoire de Bioimagerie et Pathologies UMR 7021, F-67000 Strasbourg, France

*Corresponding authors : andrey.klymchenko@unistra.fr and reisch@unistra.fr

Abstract

Efficient and safe delivery of nanoparticles (NPs) into the cytosol of living cells constitute a major challenge in bio-nanotechnology. Electroporation allows direct transfer of NPs into the cytosol by forming transient pores in the cell plasma membrane, but it is criticized for invasiveness, and the applicable particle sizes are not well defined. Here, in order to achieve efficient delivery of NPs into the cytosol with minimal cytotoxicity, we investigated the influence of the size of NPs on their electroporation and intracellular diffusion. Dye-loaded polymeric NPs with sizes between 10 and 40 nm have been prepared and coated with Tween 80. Optimizing the electroporation protocol allowed to prevent contributions of endocytosis that competes with cytosolic delivery. In this way, the effect of size on electroporation of NPs could be studied directly. We found that small NPs with 10-13 nm core diameter can be effectively delivered, which was not the case for 31-38 nm NPs, whereas 25 nm NPs showed an intermediate behavior. Taking into account the thickness of the Tween 80 shell of about 5 nm, the threshold of NP size for efficient electroporation was found to be between 18 and 30 nm. Moreover, only particles of 10-13 nm core size could diffuse freely within the entire cytosol. Finally, we showed that electroporation at excessive electric fields can directly perturb the plasma membrane leading to cytotoxicity, while the use of small NPs allows efficient delivery at relatively soft electroporation conditions. The present work provides insights into design principles for NPs and methodology for their electroporation for intracellular applications.

1. Introduction

Intracellular applications of nanoparticles (NPs), ranging from the delivery of drugs to specific compartments of the cell,[1–3] to the detection and monitoring of cellular metabolites[4–6] and to the imaging of biomolecules at the single-molecule level,[7–9] have gained increasing interest in recent years. These applications require most often the availability of the NPs directly in the cytosol. Two points are of paramount importance to achieve this: crossing the plasma membrane barrier to reach the cytosol and a high mobility within the cytosol.[10–12] Typically, NPs enter cells through endocytosis, which leads to their entrapment within endosomes.[13,14] Reaching the cytosol in this case requires to escape from the endosomal machinery, which remains challenging for NPs.[15,16] In order to circumvent this problem different approaches to access directly the cytosol have been developed that are based either on the direct permeation of the cell plasma membrane,[17] often helped by cell-penetrating peptides,[18] or using physical means to help passage across the cell membrane. Among the latter, microinjection,[19] sonoporation,[20] pinocytosis,[21] and electroporation[22] are the ones most commonly used for introducing NPs into cells.

Notably electroporation can nowadays be performed quite simply using commercially available equipment. It can be applied to various cell types, both adherent and suspended, and allows to treat a large number of cells in parallel.[23,24] In electroporation, a pulsed electric field is applied to the

medium containing the cells, inducing an additional transmembrane potential.[25,26] When the induced transmembrane potential exceeds a given threshold value, the permeation of the cell membrane is increased. This is attributed to the formation of aqueous pores in the cell membrane, initiated by the penetration of water molecules into the lipid bilayer, which causes a reorientation of the lipids and the formation of pores.[25,26] Depending on the duration and amplitude of the applied voltage pulse, pore formation can be reversible, with pore lifetimes in the range from ms to min. Electroporation can also result in the formation of irreversible pores, finally destroying the cells, which is used for tissue ablation.[26] However, in the context of delivering NPs only reversible electroporation is of interest. In particular, conditions should be optimized to achieve maximum viability and minimal perturbation of the cells following electroporation.

The resulting increased permeability of the cell plasma membrane has been used for delivery of DNA or RNA (transfection), drug delivery, and the introduction of NPs. Notably quantum dots (QDs),[21,27–29] metal (mainly Au and Ag) NPs,[30,31] but also silica NPs[32,33] have been delivered using electroporation. This brings up the question of the influence of the NP size on efficiency of delivery into the cytosol, which is probably linked to the size of the created pores.[28,32,34,35] Though NPs delivered by electroporation cover a large size range from less than 10 nm up to over 100 nm, only few examples show an actual availability of the NPs in a free form in the cytosol.[21,29] One issue is aggregation upon electroporation, which has notably been observed in the case of QDs,[27,28] but similar phenomena have also been reported for Ag NPs.[31] A second issue is the size of pores themselves vs the size of the NPs. For example, it has been shown that delivery of QDs to the cytosol requires increased voltage and pulse durations, which lead in turn to higher cytotoxicity.[29] Actual studies on the influence of the NP size on electroporation are extremely scarce and mainly concern the interaction with the cells in the earliest moments of electroporation for sizes from 30 to 70 nm.[32] Hence, there is a great need to evaluate the influence of the size on the delivery and intracellular behavior of NPs upon electroporation.

Studying both entry and intracellular behavior of NPs, depending on their size, requires a series of NPs with various sizes but sufficient brightness to be detected on the single-particle level using fluorescence microscopy. Dye-loaded polymer NPs have appeared over the last couple of years as a class of very bright fluorescent NPs.[36,37] For example, encapsulating the salt of a cationic fluorophore like hydrophobic rhodamine B derivatives with a bulky hydrophobic counterion in polymer NPs allows achieving high encapsulation, while strongly reducing aggregation induced quenching.[38,39] The resulting NPs achieve single particle brightnesses between ten to hundred times that of corresponding QDs.[11,40–42] At the same time their size can be tuned over a wide range from less than 10 to over 50 nm and they can be rendered stealth through the chemistry of the polymer and the conditions used for particle assembly,[11,12,41–44] which is important for intracellular applications. Such particles have already found various applications, including multicolor labelling of cells in vitro and in vivo,[45] single-particle tracking in cells[11,12] and mice brain,[46] oxygen sensing,[47] as well as the detection of DNA and RNA down to the single-particle and single-molecule level.[36,42,48]

In the present work, we investigated the influence of particle size on electroporation and the intracellular distribution and behavior of NPs, in order to achieve efficient delivery of dye-loaded polymer NPs into the cytosol with minimal cytotoxicity. For this we designed a series of brightly fluorescent NPs with sizes of the particle core from 10 to about 40 nm. Conditions of electroporation were optimized for these particles in order to maximize delivery through electroporation while suppressing endocytosis. The amount of delivered NPs, their intracellular distribution and mobility were studied using fluorescence microscopy with single-particle resolution. We further investigated how the electroporation parameters (electric field, pulse duration and number of pulses) needed for delivery depend on the NP size, and how to maximize particle delivery into the cytosol with minimal

cytotoxicity. The obtained results provide insights in how NP design can be used to favor an efficient and safe use of electroporation for intracellular applications of NPs.

2. Results and Discussion

Nanoparticle Size Control

In a first step, we designed a series of dye-loaded polymer NPs with different sizes through nanoprecipitation (Figure 1A). In this procedure, an organic solution (acetonitrile) containing the polymer and the dye is quickly added to a large excess of an aqueous phase. Interdiffusion of solvent and water leads to a mixture in which polymer and dye are no longer soluble, creating supersaturation, which is the driving force for particle formation.[49–51] Here, we used methyl methacrylate-based polymers (PMMA) as matrix polymers, in which we encapsulated 10 wt% (relative to the polymer) of the salt of a cationic rhodamine B derivate (R18) with a bulky hydrophobic counterion (F5-TPB) to render the NPs brightly fluorescent.[36,38]

In order to achieve a fine control over the obtained particle size, we used and combined three effects that influence particle size in nanoprecipitation: (i) Charged groups on the polymers can be used to reduce particle size, depending on their type and their fraction on the polymer.[11,41,52] Here we used PMMA bearing sulfonate groups at 1 or 2 mol % (PMMA-SO_3H). (ii) The composition, pH, and, in particular, the ionic strength of the precipitating medium can be used to further tune the effect of the charged groups on the particle size.[11,41,53] We performed nanoprecipitation in MilliQ water and in 10 and 30 mM NaCl solution. (iii) Furthermore, the particle size has been reported to increase with the concentration of the polymer in the organic phase.[41,51] Here, two polymer concentrations, 2 and 6 $g.L^{-1}$, were used. After nanoprecipitation, the NPs were stabilized with the PEG-bearing surfactant Tween 80 (T80), which has previously been shown to provide an efficient protection against protein adsorption and minimize non-specific interactions inside cells.[11,41] The resulting NPs were characterized with respect to their size using transmission electron microscopy (TEM) and dynamic light scattering (DLS) (Figure 1B, Table 1).

The combination of the different polymers and preparation conditions allowed obtaining a series of five formulations of NPs with well-defined core sizes (Figure 1B, Table 1): 10, 13, 25, 31, and 38 nm, with a quite narrow particle size distribution, according to TEM. DLS measurements of the Tween 80 treated NPs showed about 5 nm larger particle diameters, corresponding to the formation of a PEG shell around the particle core, as observed previously.[11,41] The ζ-potential of all NPs was clearly negative (between -15 and -30 mV) even after adsorption of Tween 80 (Table 1). The somewhat lower absolute ζ-values of the smaller NPs are probably due to a more efficient screening of the surface charges through the Tween shell in these NPs. The size of NPs, indicated in this work, refers to the diameter of the particle core as determined by TEM. This series of dye-loaded NPs was then used in electroporation to study the influence of NP size.

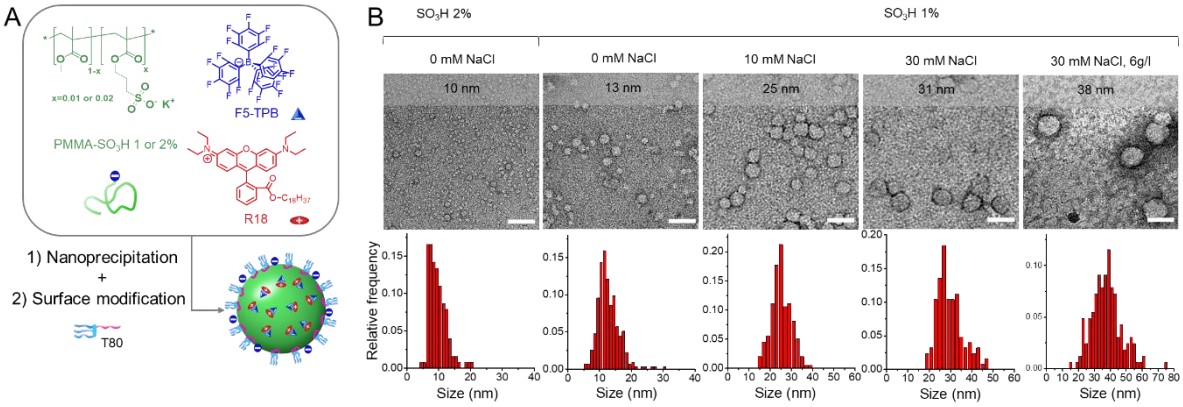

Figure 1. (A) Structures of polymers, PMMA-SO_3H 1 or 2%, dye (R18) and its counterion (F5-TPB), and scheme of preparation of dye-loaded NPs. After nanoprecipitation, the surface of particles was treated with Tween 80 (T80). (B) TEM images of dye-loaded NPs prepared from PMMA-SO_3H 1 or 2 % and different concentrations of NaCl in the aqueous phase during nanoprecipitation. All NPs were prepared from an initial polymer solution at 2 $g.L^{-1}$ except 38 nm NPs which were at a concentration of 6 $g.L^{-1}$. The size distributions are shown below the corresponding images. For each condition at least 100 NPs were measured. Scale bar: 50 nm.

Table 1. Sizes and ζ-potential of the dye-loaded NPs obtained in this study.

Polymer	[Polymer] ($g\ L^{-1}$)[a]	[NaCl] (mM)[b]	Size (nm)		ζ-potential (mV)[f]
			TEM[c]	DLS[d]	
PMMA-SO_3H 2%	2	0	10±3	14±2	-15±2
PMMA-SO_3H 1%	2	0	13±3	19±3	-21±1
PMMA-SO_3H 1%	2	10	25±5	24±4	-24±2
PMMA-SO_3H 1%	2	30	31±5	34±2	-29±2
PMMA-SO_3H 1%	6	30	38±9	46±4[e]	-27±1

[a] Concentration in the organic phase. [b] Concentration in the aqueous phase. [c] Size for bare NPs, ± gives width at half maximum. [d] For Tween 80 treated NPs, error corresponds to standard error of the mean for at least 3 measurements. [e] Without Tween 80. [f] For Tween 80 treated NPs.

Optimization of Electroporation Conditions

In a first test, we then used our 13 nm dye-loaded NPs for electroporation. For this, a solution of the NPs was mixed with a suspension of HeLa cells. Following electroporation, the cell suspension was deposited on Ibidi dishes and left to incubate at 37°C for 5 hours. Then, the cells were observed through DIC and fluorescence microscopy, in order to visualize the cells themselves and the fluorescent NPs, respectively. As a control, we used a sample that was treated exactly the same way, but without electroporation. Typical images are shown in Figure 2A: In the case of electroporated cells, a large number of fluorescent spots of different intensities and sizes are detected inside the cells. Besides, small spots, with intensities corresponding to single fluorescent NPs,[11] were present together with much brighter and larger spots. These brighter dots were also observed for the non-electroporated control samples. The latter spots can be assigned to NPs that entered the cells through endocytosis, which has already been observed for similar NPs previously.[38,45] The endocytosis of the NPs was an unwanted process, which competes with the electroporation and thus complicates the data analysis.

We optimized our electroporation protocol to decrease as much as possible the entry of NPs through endocytosis (and thus better monitor NP entry through electroporation). To achieve this, various parameters were changed, and the effects were monitored through fluorescence microscopy

and flow cytometry (Figure 2). First, we added a cell centrifugation step just after the electroporation, to separate the electroporated cells from the NPs present in the electroporation medium, and we decreased the post-electroporation rest time to 2 hours. Indeed, these two optimizations successfully decreased the signal coming from NPs entering the cell by endocytosis, but a significant amount of NPs was still present in the non-electroporated cells (SI Figures S1 and S2). Second, we investigated the influence of the electroporation medium (SI Figure S3). In particular, comparison of different electroporation media with the commercial buffer R, showed that less endocytosis but also less electroporation was observed when bringing the NPs in contact with the cells in complete DMEM medium, while Opti-MEM led to larger cell to cell variations. Furthermore, we tested Tween 80, Tween 20, and BSA, which were thought to decrease non-specific interactions between NPs and cells. Tween 80 gave the strongest reduction of endocytosis (SI Figures S2 and S4). Based on these results, we selected an following electroporation protocol (Figure 2C), in which the commercial buffer R, containing 20 $mg.L^{-1}$ of Tween 80 is used as electroporation medium; two pulses of 35 ms and a potential of 1050 V as reference parameters; and electroporation is followed by two centrifugation steps and finally by 2 h of incubation before imaging. Application of this protocol led to a nearly complete absence of fluorescence in the non-electroporated cells, and absence of bright, large spots in the electroporated cells (Figure 2A right). These results were also confirmed by flow cytometry, showing strong fluorescence signal from electroporated cells compared to the control conditions (Figure 2B).

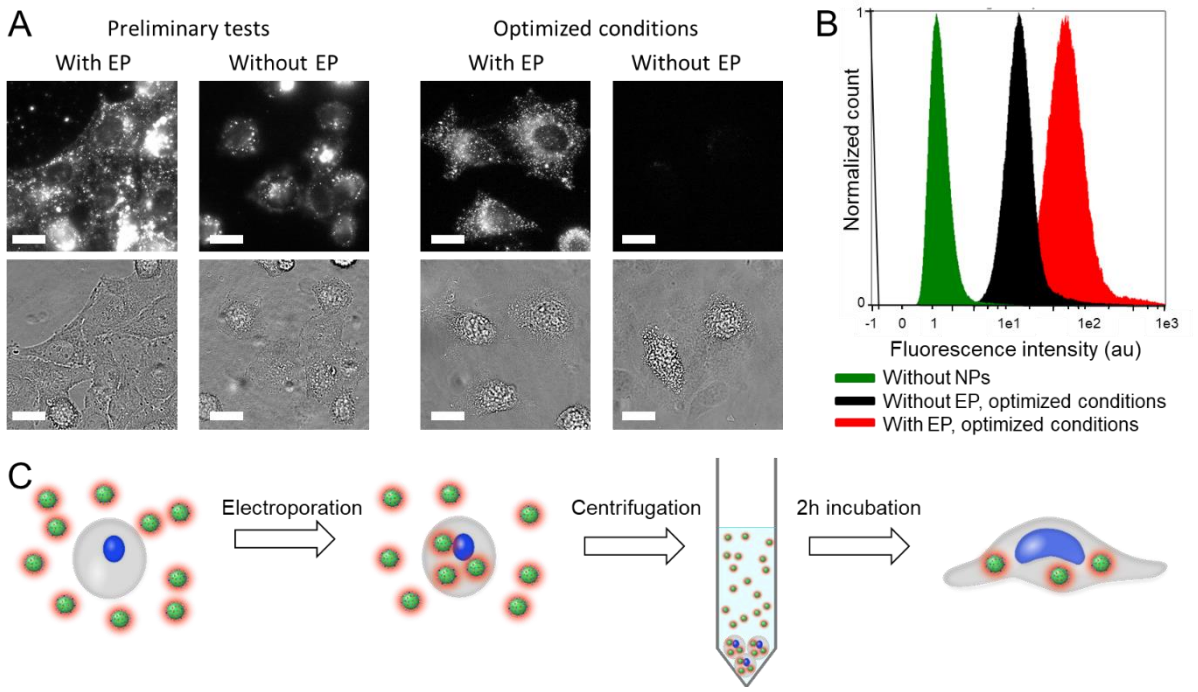

Figure 2. Optimization of conditions for electroporation. (A) Fluorescence (top) and DIC (bottom) micrographs of cells after treatment with 13 nm NPs in different conditions. Preliminary tests: NPs added to cells with and without electroporation followed by 5 h incubation. Optimized conditions: NP added to cells with and without electroporation followed by two centrifugations in the presence of Tween 80 and incubation for 2 h. Scale bars: 20 µm. (B) Flow cytometry results for cells either without NPs, or with 13 nm NPs with and without electroporation. (C) Schematic view of the adopted general protocol for electroporation of cells with NPs.

Influence of NP Size on Electroporation

We then investigated the influence of the NP size on their entry into cells upon electroporation, using our series of NPs with different sizes. All NPs were loaded with 10 wt% of the dye salt R18/F5-TPB, and, as we have shown previously, the NP size does not have a significant influence on the fluorescence quantum yield of the encapsulated dyes.[11] To directly compare the efficiency of NP entry into cells through electroporation, we thus kept the mass concentration of particles in the electroporation medium constant, and, in consequence, the overall fluorophore concentration (and overall NP fluorescence) was preserved. In this way, the amount of NPs entering the cells, in terms of mass, can be compared by measuring the overall fluorescence intensity of the treated cells, which is thus also directly proportional to the efficiency of electroporation.

Micrographs of cells after electroporation with NPs of different sizes are shown in Figure 3A. In all cases, using our optimized electroporation protocol, fluorescence essentially appeared as separated spots. In the case of 10 and 13 nm NPs, a high number of spots, attributed to individual NPs,[40] was observed in all cells. In the case of 25 nm NPs, the number of fluorescent spots decreased dramatically. For 31 and 38 nm NPs, only very rare spots were detected inside cells. Cellular images were then used to quantitatively compare the efficiency of NP entry through electroporation depending on the particle size. For this, the average total fluorescence intensity per cell was analyzed for at least 20 cells per condition (Figure 3B): For 10 and 13 nm NPs the intracellular fluorescence signal was similarly strong, whereas for 25 nm NPs it dropped nearly 4-fold. For 31 and 38 nm NPs a further decrease of the signal was observed.

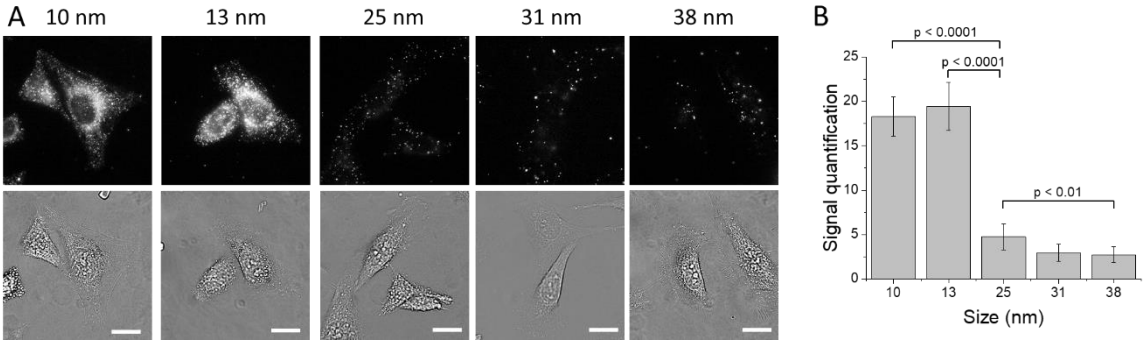

Figure 3. NP size and internalization through electroporation. (A) Fluorescence (top) and DIC (bottom) micrographs of cells electroporated with NPs of 5 different sizes using the optimized protocol, 2 h after electroporation. Scale bar: 20 µm. (B) Average fluorescence intensity per cell obtained for the different NP sizes. At least 20 cells per condition were evaluated. Error bars correspond to standard errors of the mean. The mass concentration of NPs, and thus the overall fluorescence, was kept constant in the electroporation medium.

The mobility of the NPs inside the cytosol, and notably their capacity to reach all regions inside the cell, is of prime importance for most intracellular sensing, delivery, and imaging applications. In a further step, we hence analyzed the movement of NPs of different sizes inside the cells after electroporation. A qualitative comparison can be made by observing directly the movement and distribution of the NPs in the cytosol (SI videos) and from the maximum projections of the particle intensities over a given time (here 36 s, Figure 4 A). The 10 and 13 nm NPs were found to be distributed throughout the entire cell, and practically all NPs were mobile. 25-nm NPs were still found all over the cell. However, about half of the observed fluorescent spots did not show significant movement over the time of experiments. Spreading and movement were much less expressed for the larger NPs (31 and 38 nm).

To obtain a more quantitative picture, we then applied single-particle tracking to the NPs after electroporation, which is facilitated by the high fluorescence brightness of our dye-loaded NPs. The

conditions and, in particular, the NP concentration in the electroporation medium were adjusted so as to obtain between 10 and 40 NPs per cell, in order to facilitate tracking (SI Figure S5). Plotting mean square displacement (MSD) vs lag time for the individual trajectories allows to analyze the intracellular behavior of particles (Figure 4 B).[54,55] For 10 and 13 nm NPs, a linear increase of the MSD vs lag time was observed over a wide time scale. Such a behavior indicates normal Brownian diffusion of the NPs. Starting from 25 nm NPs, the MSD deviated from linearity already for relatively low lag times, indicating restricted diffusion of such NPs. The initial slope of the MSD curves was used to estimate the diffusion coefficients of the different NPs (Figure 4, SI Figure S6). The smaller 10 and 13 nm NPs showed mean diffusion coefficients of the order of 0.9 $\mu m^2\ s^{-1}$, in good agreement with previous results for NPs in free movement inside the cytosol.[10–12] For 25 nm NPs the mean diffusion coefficient dropped to less than 0.3 $\mu m^2\ s^{-1}$, and a further decrease was observed for the larger NPs. In these cases, some NPs still had a quite high mobility, these probably corresponded to the smallest NPs (<25 nm) of the distributions (see TEM data, Figure 1B).

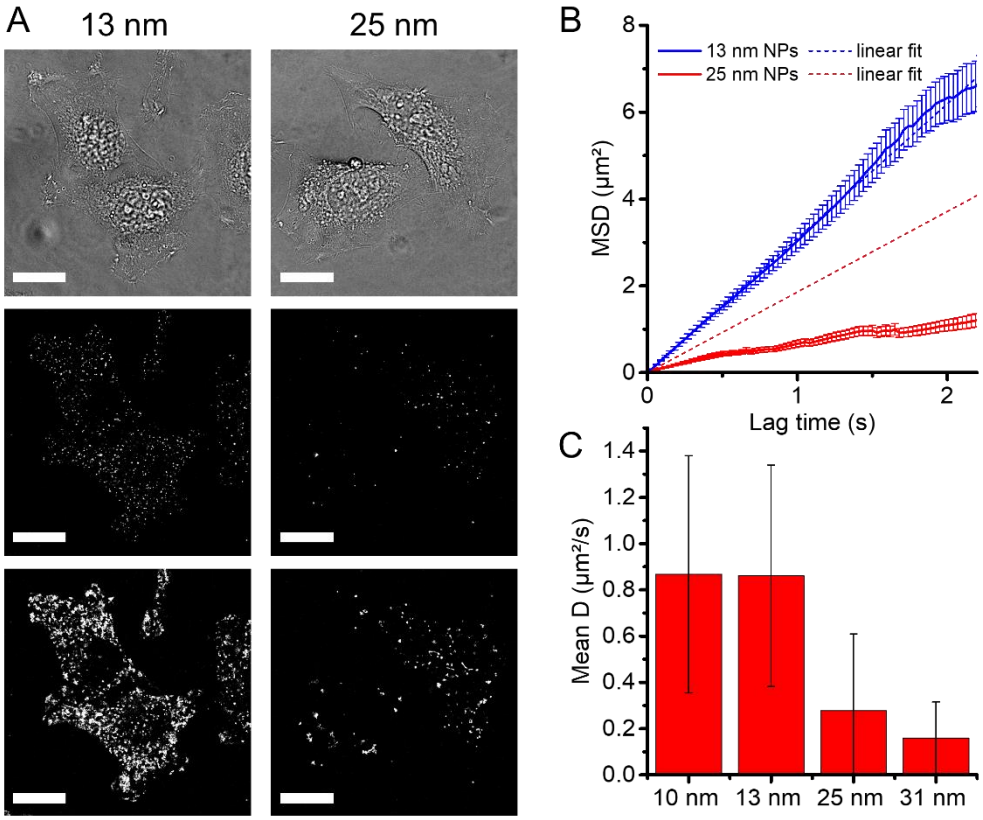

Figure 4. Single-particle imaging and tracking of NPs of different sizes inside cells after electroporation. (A) Micrographs of HeLa cells electroporated with NPs of mean size 13 (left) and 25 nm (right), respectively, loaded with 10 wt% R18/F5-TPB and stabilized with Tween 80. Top: DIC micrographs. Middle: instantaneous fluorescence micrographs. Bottom: Maximum projection of fluorescence over 36 s. Scale bars correspond to 20 µm. (B) Mean square displacement (MSD) vs lag time for 13 and 25 nm NPs. Solid curves correspond to the mean MSD for at least 70 trajectories; dashed lines are linear fits based on the first 5 points; error bars correspond to SD/√N. (C) Mean diffusion coefficients for NPs of different sizes inside cells after electroporation. At least 30 trajectories were analyzed per condition. Error bars give standard deviation over all trajectories.

Safe Electroporation and NP Size

Even with up-to-date equipment electroporation remains a quite invasive procedure, as its aim is to perturb the cell membrane and create pores. Cytotoxicity of electroporation notably depends on the electric field strength and pulse length, that determine to which extent pore formation is reversible.[26] At the same time, these parameters also correlate with the size of the created pores.[35] Efficient electroporation of NPs has been reported to require increased pulse amplitude and length, compared to small molecules, due to the need for larger pores.[29] We hence wanted to evaluate how decreasing the particle size leads to a situation in which "softer" electroporation conditions are sufficient to introduce NPs into the cytosol. On the other hand, we wanted to understand to which extent the conditions of electroporation can contribute to the cytotoxicity of the protocol.

First, we evaluated the impact of different electroporation conditions on HeLa cells in two ways: (1) Cell viability was quantified using a WST1 assay, an analogue of the MTT assay, 18 h after electroporation (Figure 5 A). For our reference conditions, 1050 V in two 35 ms pulses, cell viability was only slightly reduced to 92%, compared to non-electroporated cells. When reducing the applied potential to 750 V, the viability was within 95%. However, when the potential was increased to 1200 V, viability dropped to 26%, indicating a clear cytotoxicity of electroporation towards HeLa cells under these conditions. (2) Perturbations of the cellular membrane were analyzed using fluorescently labelled Annexin V as probe. Annexin V has a strong affinity for phosphatidylserine, which is normally restricted to the inner leaflet of the cell membrane. Apoptosis or direct perturbation of the cell plasma membrane leads to exposure of phosphatidylserine at the outer cell surface, which can be detected by fluorescently labelled Annexin V.[56] Here, we used it as a probe indicating the extent of membrane perturbation after electroporation, by performing the assay directly after electroporation and analyzing it through flow cytometry. For non-electroporated cells and those electroporated with 750 and 1050 V, about 12% of Annexin V positive cells were detected. However, when increasing the potential to 1200 V, 45% of cells became Annexin V positive. This indicates that under the reference conditions used here, very little membrane disorganization occurs or it is quickly reversible, whereas harsher electroporation conditions have a quite strong direct effect on the plasma membrane.

We then investigated how the entry of NPs into cells depends on the electroporation conditions, notably in view of softer electroporation, by decreasing the potential or pulse length. For 13 nm NPs, decreasing the applied potential led to a significant decrease in the number of particles per cell, with about 40% particles at 900 V and 20% at 750 V, compared to 1050 V (Figure 5 C, SI Figure S7). A similar decrease in particle number was found when the pulse length was decreased from 35 to 20 and 10 ms. However, the interesting point was that even at the softest electroporation conditions we still observed a quite large number of particles per cell (e.g. of the order of 20 - 40 particles per cell for 750 V), which is well suited for single-particle tracking. More importantly, most of these particles were highly mobile (Figure 5 B, Supporting Videos), suggesting that such small NPs can be readily delivered into the cytosol using these very soft electroporation conditions, far below the cytotoxicity threshold. We conducted the same experiments with 38 nm as negative control. In this case, decreasing the potential further decreased the already very low entry of NPs, and virtually no particles were detected inside cells at 750 V. These results suggest that soft electroporation conditions, while being relatively efficient for small NPs, do not allow delivery of larger NPs into the cytosol.

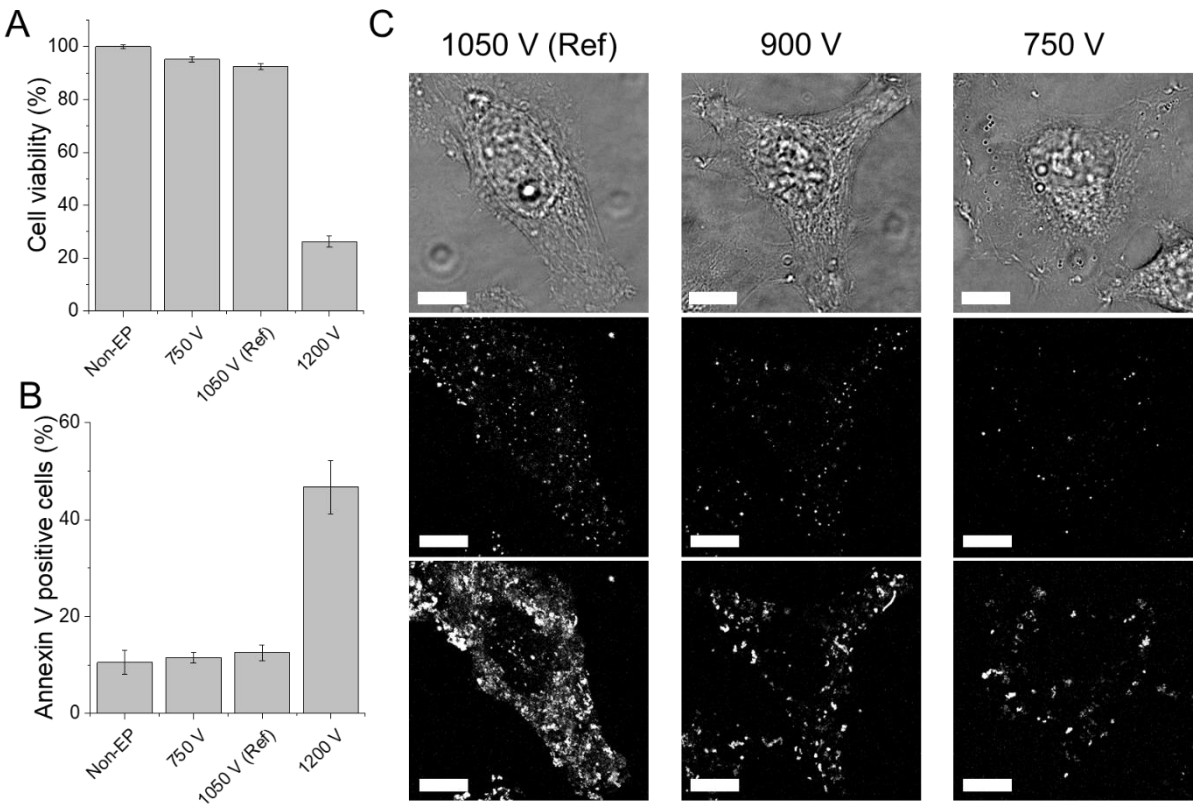

Figure 5. Conditions of electroporation and their influence on cells and entry of NPs. (A) Quantification of cell viability using the WST1 assay after 18h of rest and (B) evaluation of cell membrane perturbations with Annexin V by flow cytometry, 10 min after electroporation. (C) Micrographs of cells electroporated using different pulse intensities with 13 nm NPs, and at 750 V with 38 nm NPs. Top: DIC, Middle: Instantaneous fluorescence image; Bottom: Maximum projections over 36 s. Scale bars: 10 µm.

Discussion

In order to optimize NP design in view of efficient delivery into the cytosol, we have studied here electroporation of NPs of different size (10-40 nm) in live cells and their intracellular single-particle behavior. In particular, we focused on the influence of particle size in terms of entry and availability in free form of the NPs in the cytosol as well as on optimization of electroporation conditions to minimize cytotoxicity.

A first challenge was to develop an electroporation method that largely favored electroporation over endocytosis. The key points that led to significant improvements were removal of non-electroporated NPs through centrifugation, and a proper choice of the medium used for electroporation to avoid particle binding to the cells. Preventing endocytosis of NPs allowed us to study the influence of particle size on electroporation.

We then compared the electroporation efficiencies of NPs of different sizes in terms of mass transfer rates at equal particle mass concentration using fluorescence microscopy (it has to be noted that in consequence the number concentrations are different). From our experiments, we could clearly distinguish two size ranges: NPs with average diameters of 10 and 13 nm entered the cells easily upon electroporation and showed a very high mobility inside the cytosol. NPs of 31 and 38 nm, on the other hand, showed only very limited entry and the ones that were found inside cells had a very low mobility. NPs with an average diameter of 25 nm showed an intermediate behavior, with still a detectable entry

of NPs. About half of these NPs had a relatively high mobility, while others were found to be practically immobile.

We suppose that two phenomena are at the origin of the size dependence of the cytosol delivery of NPs and their intracellular mobility. On the one hand, only NPs that are smaller than the pores formed during electroporation can enter directly the cytosol. On the other hand, only NPs below a certain size can move freely in the crowded intracellular environment.[57,58] For the latter, we previously found a critical core size of about 23 nm for free diffusion of dye-loaded polymer NPs after microinjection.[11] This is in line with other studies on the intracellular mobility of NPs,[10] and it is confirmed by the results we obtained here on single-particle diffusion. Indeed, the 10 and 13 nm NPs showed a high mobility with diffusion coefficients close to 1 $\mu m^2 s^{-1}$. Only a part of the 25 nm NPs showed still a relatively high mobility, probably corresponding to the smaller particles of the distribution. Larger particles (>25 nm) displayed only a very low mobility.

The observed size dependence of electroporation allows further to establish the size cut-off for entry through the pores formed during electroporation. Under standard electroporation conditions (1050 V, 35 kV m^{-1},2x 35 ms pulses), we observed a threshold between 13 and 25 nm of core particle size for accessing the intracellular medium. This is supported by the fact that very small number of NPs of 31 and 38 nm diameter were detected after electroporation. A closer observation of the particle size distributions (Figure 1B) suggests that the signal obtained for the 25 nm NPs inside the cells corresponds to the smallest particles of the distribution, which can be as small as 15 nm. Considering a 5-nm Tween 80 shell, the cut-off size of NPs in our electroporation conditions, in terms of hydrodynamic diameter, is in the range 18-30 nm. Together these results indicate that the largest pores formed during electroporation, which have a sufficient lifetime for NPs to pass, are of the order of 30 nm. This is in line with early estimations of pore sizes using large macromolecules (dextrans), for which pore sizes of close to 10 nm were obtained,[59–61] and other study suggesting that transiently larger pores can be formed.[62]

A further insight into the possibilities and limits of electroporation for NPs could be obtained here by varying the electroporation conditions, i.e. the potential and the duration of the pulses. On the one hand, increasing the voltage to 1200 V quickly led to strong perturbations of the cell plasma membrane, as indicated by an increased Annexin V labelling, and finally resulted in high cytotoxicity. On the other hand, decreasing the potential and pulse duration also decreased the efficiency of delivery of smaller NPs. However, even at the lowest potential and pulse durations used here (750 V; and 10 ms) a significant amount of 13 nm NPs could still be successfully delivered into the cytosol, while preserving their high mobility. The obtained results are in line with simulations showing that the pore sizes increase with applied potential and duration.[35] This means that there is an upper threshold of particle sizes that can be safely delivered directly to the cytosol, lying between 25 and 30 nm. Furthermore, it also shows the benefits of very small NPs with core sizes < 15 nm, as they can still be delivered to cells under very soft electroporation conditions far below the cytotoxic threshold.

Together, the results obtained here indicate that delivery of NPs in a free form into the cytosol requires NPs with hydrodynamic diameters below 30 nm diameter, and ideally below 20 nm (core size <15 nm). Indeed, only these NPs can be efficiently delivered into the cytosol without strong perturbations of the cells, and at the same time are small enough to diffuse freely and reach all the regions of the cytosol.

3. Conclusions

In the present work, we investigated the influence of the size of NPs for efficient delivery into the cytosol of living cells in a free form using electroporation. To achieve this, we designed a series of dye-loaded polymer NPs with well-defined core sizes ranging from 10 to 40 nm by varying the amount of

charged groups on the polymers and the conditions used for nanoprecipitation. After optimization of the electroporation protocol to minimize endocytosis, we then used this series of NPs for electroporation. Evaluation of electroporation efficiency using fluorescence microscopy and of intracellular diffusion using single-particle tracking, revealed a threshold between 18 and 30 nm of the particle hydrodynamic diameter for efficient delivery in a free form to the cytosol. Thus, a further reduction of the particle size to less than 20 nm is advantageous for the delivery of NPs to the cytosol using very soft electroporation conditions, minimizing perturbations of cells. The presented results give clear guidelines to the design of particles intended for the use in intracellular applications and for their safe delivery using electroporation.

4. Materials and methods

Materials

Poly(methyl methacrylate-co-3-sulfopropyl methacrylate) polymers (PMMA-SO_3H 1 or 2 %) were synthetized through free radical polymerization as described previously.[11,12,43] R18/F5-TPB was synthesized from rhodamine B octadecyl ester perchlorate (Sigma-Aldrich, >98.0%) and lithium tetrakis(pentafluorophenyl)borate ethyl etherate (Alfa Aesar, 97%) through ion exchange followed by purification through column chromatography according to the method previously described.[38,45] Milli-Q water (Millipore), NaCl (≥98%, Sigma-Aldrich), acetonitrile (≥99.9%, Sigma-Aldrich) and Tween 80 (T80, Polysorbate 80, Sigma-Aldrich) were used for preparation of NPs.

Methods

Preparation of NPs

Stock solutions of polymers were prepared at a concentration of 10 $g.L^{-1}$ in acetonitrile. These solutions were diluted to 2 or 6 $g.L^{-1}$ in acetonitrile containing 10 wt% of R18/F5-TPB (relative to the polymer). This solution was quickly added to a 10-fold volume excess of water or NaCl solution (at 10 or 30 x 10^{-3} M) under shaking (Thermomixer comfort, Eppendorf, 1000 rpm at 21°C), followed by a second dilution in water. The latter solution was further diluted to obtain the desired NP concentrations and Tween 80 was added to obtain a final concentration of 0.05 $g.L^{-1}$.

Characterization of NPs

Transmission electron microscopy (TEM). Solutions of bare dye-loaded NPs (5µL) were deposited onto carbon-coated copper−rhodium electron microscopy grids following amylamine glow-discharge. They were then treated for 20 s with a 2% uranyl acetate solution for staining. The obtained grids were observed using a Philips CM120 transmission electron microscope equipped with a LaB6 filament and operating at 100 kV. The acquisition of areas of interest was recorded with a Peltier-cooled CCD camera (model 794, Gatan, Pleasanton, CA). Images were analyzed using the Fiji software. At least 200 particles per condition were analyzed.

Dynamic light scattering (DLS) and ζ–potential. The size and ζ–potential of Tween 80 treated dye-loaded NPs were measured on a Zetasizer Nano series ZSP (Malvern Instruments S.A.). For size determination, each sample was measured 10 times with a run length of 10 s each. The volume average values were used, which are determined by the Zetasizer software (Malvern) based on Mie theory. Mean values give the average over at least three independent measurements, error bars correspond to standard error of the mean. For ζ–potential determination three successive measurements combining electrophoretic mobility and Laser Doppler Velocimetry with > 10 runs each were carried out with an applied potential of ±150 V.

Cell Culture

Hela cells (ATCC® CCL-2) were grown in Dulbecco's modified Eagle's medium with low (1 $g.L^{-1}$) glucose (DMEM, Gibco), supplemented with 10% fetal bovine serum (FBS, Dutscher), 1% L-glutamine (Lonza) and 1% penicillin-streptomycin (Lonza) at 37°C in a humidified atmosphere containing 5% CO_2.

Electroporation

On the day of electroporation, Hela cells were detached with Trypsin (Lonza), centrifuged at 1300 rpm during 5 min, counted, and finally washed one time with DPBS (Dutscher). The electroporation was then carried out using a Neon Transfection System (Invitrogen), which is a capillary electroporation system with a wire type electrode,[63] as described in the instruction manual in 100 µL volumes. In brief, 500 000 cells were resuspended in Buffer R, electroporated and finally put in µ-Dishes (Ibidi, 35 mm, 2 mL) and let to recover for a given time before the observations by microscopy. To optimize the electroporation protocol to deliver NPs, multiple parameters including type of contact buffer, with a centrifugation just after electroporation, time of rest and conditions of electroporation themselves (voltage, number of pulse, width) were tested as described in the results section. The reference conditions for electroporation were 2 pulses of 1050 V with a width of 35 ms and a repetition rate of 1 s^{-1}. The electric field associated with the potentials used here can be estimated to : 750 V : 25 kV m^{-1}; 900 V : 30 kV m^{-1}; 1050 V : 35 kV m^{-1}; 1200 V : 40 kV m^{-1}.[63]

Cell Imaging

For imaging, the medium was removed and the attached cells were washed once with complete medium without antibiotics and incubated in this same medium for the observations. Two microscope set-ups were used for observation: (1) For general visualization of the NPs, images were acquired in epi-fluorescence mode with a Nikon Ti-E inverted microscope which was equipped with CFI Plan Apo ×60 oil (Nikon, NA = 1.4) objective, and a Orca Flash 4 sCMOS camera (Hamamatsu). Excitation was performed at 550 nm with an LED Spectra X (Lumencor) at a nominal power of 10%, and the emission was recorded from 555 to 635 nm and an exposure time of 50 ms per image frame. The images were recorded using NIS Elements and then processed with ImageJ. (2) For single particle tracking, measurements were performed in the TIRF (total internal reflection fluorescence) or HILO mode on a homemade wide-field setup based on an Olympus IX-71 microscope with an oil immersion objective (NA = 1.49, 100×). A DPPS (Cobolt) continuous-wave laser emitting at 532 nm was used for excitation at 5 W/cm^2. The fluorescence signal was recorded with an EMCCD (ImagEM Hamamatsu) using an exposure time of 30.5 ms per image frame.

Image Analysis and Quantification

Image analysis was performed using the ImageJ software. The quantification of signal was performed for at least 20 cells per condition.

For tracking nanoparticles, the trajectories were obtained using the TrackMate plugin for Fiji.[64] Then, MSD curves were plotted and slopes extracted from the MSD curves with a MATLAB script for the particle tracking analysis.

Flow Cytometry

Flow cytometry was performed with a MACSQuant® VYB (Miltenyi Biotec). Gates were defined to select live cells by forward (FSC) and side scatter channels (SSC). At least 10 000 events were collected for each condition for analysis on the MACSQuantify™ Software. To detect the rhodamine B signal emitted by NPs a 561 nm laser (100 mW) was used for excitation and the emission captured through a 651/671 nm band pass filter. For Annexin V assays a 480 nm or 561 nm laser were used for excitation, as detailed below.

Annexin V Assay

For the evaluation of cell perturbations, Hela cells were detached from the flask more softly with a solution of Accutase (Stemcell) instead of trypsin. After the electroporation, cells were directly washed in cold DPBS (Dutscher). Cells were then centrifuged for 5 min at 1300 rpm and resuspended in annexin-binding buffer (10 mM HEPES; 140 mM NaCl; 2,5 mM $CaCl_2$; pH 7.4) at a cell concentration of ~ 1×10^6 cells/mL. Then, 5 µL of the annexin V -Alexa Fluor 488 or 561 nm (ThermoFisher) were added for each 100 µL of cell suspension. Finally, the mixture was incubated for 15 min at RT, followed by an addition of 400 µL of annexin-binding buffer. Samples were kept on ice until the flow cytometry acquisition (488 nm, 50mW or 561 nm, 100 mW, lasers, and emission captured through a 500/550 nm or 651/671 nm band pass filter respectively. All experiments were repeated three times.

Cell Proliferation Analysis

The Cell Proliferation Reagent WST-1 (Merck) was used for the cell proliferation analysis. After the different conditions of electroporation, Hela cells were seeded in a 96 well plate with a density of 1×10^4 cells/ well and incubated overnight. Then, 5 µL/well of WST-1 were applied and the 96 well plate was incubated for 1h at 37°C in 5% CO_2. After 1 h of incubation, viability was monitored by measuring the absorbance at 450 nm with the reference wavelength set at 655 nm using an iMark™ Microplate Absorbance Reader (Biorad). The viability of the control cells without electroporation was set as 100%. All tests were performed in triplicate.

Acknowledgements

This work was supported by the European Research Council ERC Consolidator grant BrightSens 648528 and Agence National de Recherche JC/JC grant “Supertrack” ANR-16-CE09-0007. The authors thank C. Crucifix from the FRISBI platform (ANR-10-INBS-05) for help with electron microscopy and Frédéric Przybilla for help with single particle tracking analysis.

5. References

[1] P. Gao, W. Pan, N. Li, B. Tang, *ACS Appl. Mater. Interfaces* **2019**, *11*, 26529.
[2] C. P. Cerrato, K. Künnapuu, Ü. Langel, *Expert Opin. Drug Deliv.* **2017**, *14*, 245.
[3] W.-H. Chen, G.-F. Luo, X.-Z. Zhang, *Adv. Mater.* **2019**, *31*, 1802725.
[4] C. Ding, A. Zhu, Y. Tian, *Acc. Chem. Res.* **2014**, *47*, 20.
[5] P. Zrazhevskiy, M. Sena, X. Gao, *Chem. Soc. Rev.* **2010**, *39*, 4326.
[6] A. Mokhtarzadeh, H. Vahidnezhad, L. Youssefian, J. Mosafer, B. Baradaran, J. Uitto, *Trends Mol. Med.* **2019**, *25*, 1066.
[7] A. Kusumi, T. A. Tsunoyama, K. M. Hirosawa, R. S. Kasai, T. K. Fujiwara, *Nat. Chem. Biol.* **2014**, *10*, 524.
[8] F. Pinaud, S. Clarke, A. Sittner, M. Dahan, *Nat. Methods* **2010**, *7*, 275.
[9] P. Pierobon, G. Cappello, *Adv. Drug Deliv. Rev.* **2012**, *64*, 167.
[10] F. Etoc, E. Balloul, C. Vicario, D. Normanno, D. Liße, A. Sittner, J. Piehler, M. Dahan, M. Coppey, *Nat. Mater.* **2018**, *17*, 740.
[11] A. Reisch, D. Heimburger, P. Ernst, A. Runser, P. Didier, D. Dujardin, A. S. Klymchenko, *Adv. Funct. Mater.* **2018**, *28*, 1805157.
[12] A. Runser, D. Dujardin, P. Ernst, A. S. Klymchenko, A. Reisch, *ACS Appl. Mater. Interfaces* **2020**, *12*, 117.
[13] G. Sahay, D. Y. Alakhova, A. V. Kabanov, *J. Controlled Release* **2010**, *145*, 182.
[14] P. Foroozandeh, A. A. Aziz, *Nanoscale Res. Lett.* **2018**, *13*, 339.
[15] K. E. Sapsford, W. R. Algar, L. Berti, K. B. Gemmill, B. J. Casey, E. Oh, M. H. Stewart, I. L. Medintz, *Chem. Rev.* **2013**, *113*, 1904.
[16] S. A. Smith, L. I. Selby, A. P. R. Johnston, G. K. Such, *Bioconjug. Chem.* **2019**, *30*, 263.
[17] H. Nakamura, S. Watano, *KONA Powder Part. J.* **2018**, *35*, 49.
[18] E. Derivery, E. Bartolami, S. Matile, M. Gonzalez-Gaitan, *J. Am. Chem. Soc.* **2017**, *139*, 10172.
[19] P. Tiefenboeck, J. A. Kim, J.-C. Leroux, *Adv. Drug Deliv. Rev.* **2018**, *132*, 3.
[20] I. Lentacker, I. De Cock, R. Deckers, S. C. De Smedt, C. T. W. Moonen, *Adv. Drug Deliv. Rev.* **2014**, *72*, 49.
[21] E. Muro, A. Fragola, T. Pons, N. Lequeux, A. Ioannou, P. Skourides, B. Dubertret, *Small* **2012**, *8*, 1029.
[22] K. Kim, W. G. Lee, *J. Mater. Chem. B* **2017**, *5*, 2726.
[23] H. Nakamura, J. Funahashi, *Dev. Growth Differ.* **2013**, *55*, 15.
[24] J. Shi, Y. Ma, J. Zhu, Y. Chen, Y. Sun, Y. Yao, Z. Yang, J. Xie, *Molecules* **2018**, *23*, 3044.
[25] J. Gehl, *Acta Physiol. Scand.* **2003**, *177*, 437.
[26] M. L. Yarmush, A. Golberg, G. Serša, T. Kotnik, D. Miklavčič, *Annu. Rev. Biomed. Eng.* **2014**, *16*, 295.
[27] J. B. Delehanty, H. Mattoussi, I. L. Medintz, *Anal. Bioanal. Chem.* **2009**, *393*, 1091.
[28] T. Batista Napotnik, D. Miklavčič, *Bioelectrochemistry* **2018**, *120*, 166.
[29] C. Sun, Z. Cao, M. Wu, C. Lu, *Anal. Chem.* **2014**, *86*, 11403.
[30] Y. Zu, S. Huang, W.-C. Liao, Y. Lu, S. Wang, *J. Biomed. Nanotechnol.* **2014**, *10*, 982.
[31] J. Lin, R. Chen, S. Feng, Y. Li, Z. Huang, S. Xie, Y. Yu, M. Cheng, H. Zeng, *Biosens. Bioelectron.* **2009**, *25*, 388.
[32] K. Kim, J. A. Kim, S.-G. Lee, W. G. Lee, *Nanoscale* **2012**, *4*, 5051.
[33] T. Kim, E. Momin, J. Choi, K. Yuan, H. Zaidi, J. Kim, M. Park, N. Lee, M. T. McMahon, A. Quinones-Hinojosa, J. W. M. Bulte, T. Hyeon, A. A. Gilad, *J. Am. Chem. Soc.* **2011**, *133*, 2955.
[34] A. E. Sowers, M. R. Lieber, *FEBS Lett.* **1986**, *205*, 179.
[35] W. Krassowska, P. D. Filev, *Biophys. J.* **2007**, *92*, 404.
[36] A. Reisch, A. S. Klymchenko, *Small* **2016**, *12*, 1968.
[37] K. Li, B. Liu, *Chem. Soc. Rev.* **2014**, *43*, 6570.
[38] A. Reisch, P. Didier, L. Richert, S. Oncul, Y. Arntz, Y. Mély, A. S. Klymchenko, *Nat. Commun.* **2014**, *5*, 4089.
[39] B. Andreiuk, A. Reisch, E. Bernhardt, A. S. Klymchenko, *Chem. – Asian J.* **2019**, *14*, 836.

[40] A. Reisch, K. Trofymchuk, A. Runser, G. Fleith, M. Rawiso, A. S. Klymchenko, *ACS Appl. Mater. Interfaces* **2017**, *9*, 43030.
[41] A. Reisch, A. Runser, Y. Arntz, Y. Mély, A. S. Klymchenko, *ACS Nano* **2015**, *9*, 5104.
[42] N. Melnychuk, A. S. Klymchenko, *J. Am. Chem. Soc.* **2018**, *140*, 10856.
[43] V. Rosiuk, A. Runser, A. Klymchenko, A. Reisch, *Langmuir* **2019**, *35*, 7009.
[44] M. Cardoso Dos Santos, A. Runser, H. Bartenlian, A. M. Nonat, L. J. Charbonnière, A. S. Klymchenko, N. Hildebrandt, A. Reisch, *Chem. Mater.* **2019**, *31*, 4034.
[45] B. Andreiuk, A. Reisch, M. Lindecker, G. Follain, N. Peyriéras, J. G. Goetz, A. S. Klymchenko, *Small* **2017**, *13*, 1701582.
[46] I. Khalin, D. Heimburger, N. Melnychuk, M. Collot, B. Groschup, F. Hellal, A. Reisch, N. Plesnila, A. S. Klymchenko, *ACS Nano* **2020**.
[47] P. Ashokkumar, N. Adarsh, A. S. Klymchenko, *Small* **2020**, *16*, 2002494.
[48] N. Melnychuk, S. Egloff, A. Runser, A. Reisch, A. S. Klymchenko, *Angew. Chem. Int. Ed.* **2020**, *59*, 6811.
[49] C. J. Martínez Rivas, M. Tarhini, W. Badri, K. Miladi, H. Greige-Gerges, Q. A. Nazari, S. A. Galindo Rodríguez, R. Á. Román, H. Fessi, A. Elaissari, *Int. J. Pharm.* **2017**, *532*, 66.
[50] W. S. Saad, R. K. Prud'homme, *Nano Today* **2016**, *11*, 212.
[51] E. Lepeltier, C. Bourgaux, P. Couvreur, *Adv. Drug Deliv. Rev.* **2014**, *71*, 86.
[52] C. Zhang, V. J. Pansare, R. K. Prud'homme, R. D. Priestley, *Soft Matter* **2011**, *8*, 86.
[53] K. Trofymchuk, A. Reisch, P. Didier, F. Fras, P. Gilliot, Y. Mely, A. S. Klymchenko, *Nat. Photonics* **2017**, *11*, 657.
[54] C. D. Rienzo, E. Gratton, F. Beltram, F. Cardarelli, *Proc. Natl. Acad. Sci.* **2013**, *110*, 12307.
[55] N. Ruthardt, D. C. Lamb, C. Bräuchle, *Mol. Ther.* **2011**, *19*, 1199.
[56] S. J. Martin, C. P. Reutelingsperger, A. J. McGahon, J. A. Rader, R. C. van Schie, D. M. LaFace, D. R. Green, *J. Exp. Med.* **1995**, *182*, 1545.
[57] K. Luby-Phelps, *Mol. Biol. Cell* **2013**, *24*, 2593.
[58] T. Kalwarczyk, K. Sozanski, A. Ochab-Marcinek, J. Szymanski, M. Tabaka, S. Hou, R. Holyst, *Adv. Colloid Interface Sci.* **2015**, *223*, 55.
[59] Y. Rosemberg, R. Korenstein, *Biophys. J.* **1990**, *58*, 823.
[60] M. T. Hood, C. Stachow, *Appl. Environ. Microbiol.* **1992**, *58*, 1201.
[61] S. Yumura, R. Matsuzaki, T. Kitanishi-Yumura, *Cell Struct. Funct.* **1995**, *20*, 185.
[62] D. A. Zaharoff, J. W. Henshaw, B. Mossop, F. Yuan, *Exp. Biol. Med.* **2008**.
[63] J. A. Kim, K. Cho, M. S. Shin, W. G. Lee, N. Jung, C. Chung, J. K. Chang, *Biosens. Bioelectron.* **2008**, *23*, 1353.
[64] J.-Y. Tinevez, N. Perry, J. Schindelin, G. M. Hoopes, G. D. Reynolds, E. Laplantine, S. Y. Bednarek, S. L. Shorte, K. W. Eliceiri, *Methods* **2017**, *115*, 80.